Insight into the Ligand-Mediated Synthesis of Colloidal CsPbBr₃ Perovskite Nanocrystals: The Role of Organic Acid, Base, and Cesium Precursors

Aizhao Pan,[†,‡] Bo He,[‡,⊥] Xiaoyun Fan,[‡,§] Zeke Liu,[∥] Jeffrey J. Urban,[‡] A. Paul Alivisatos,[⊥,∥] Ling He,[*,†] and Yi Liu[*,‡,⊥]

[†]Department of Chemistry, School of Science, Xi'an Jiaotong University, Xianning West Road, 28, Xi'an, 710049, China

[‡]The Molecular Foundry and [⊥]Materials Sciences Division, Lawrence Berkeley National Laboratory, Berkeley, California 94720, United States

[§]Xinjiang Key Laboratory of Electronic Information Materials and Devices, Xinjiang Technical Institute of Physics & Chemistry, Chinese Academy of Sciences, Urumqi 830011, China

[∥]Department of Chemistry, University of California, Berkeley, and Kavli Energy NanoSciences Institute at Berkeley, Berkeley, California 94720, United States

Ⓢ *Supporting Information*

ABSTRACT: While convenient solution-based procedures have been realized for the synthesis of colloidal perovskite nanocrystals, the impact of surfactant ligands on the shape, size, and surface properties still remains poorly understood, which calls for a more detailed structure−morphology study. Herein we have systematically varied the hydrocarbon chain composition of carboxylic acids and amines to investigate the surface chemistry and the independent impact of acid and amine on the size and shape of perovskite nanocrystals. Solution phase studies on purified nanocrystal samples by ¹H NMR and IR spectroscopies have confirmed the presence of both carboxylate and alkylammonium ligands on surfaces, with the alkylammonium ligand being much more mobile and susceptible to detachment from the nanocrystal surfaces during polar solvent washes. Moreover, the chain length variation of carboxylic acids and amines, ranging from 18 carbons down to two carbons, has shown independent correlation to the size and shape of nanocrystals in addition to the temperature effect. We have additionally demonstrated that employing a more soluble cesium acetate precursor in place of the universally used Cs₂CO₃ results in enhanced processability without sacrificing optical properties, thus offering a more versatile recipe for perovskite nanocrystal synthesis that allows the use of organic acids and amines bearing chains shorter than eight carbon atoms. Overall our studies have shed light on the influence of ligand chemistry on crystal growth and stabilization of the nanocrystals, which opens the door to functionalizable perovskite nanocrsytals through surface ligand manipulation.

**KEYWORDS:** colloidal nanocrystal, nanocubes, nanoplatelets, perovskite, surface chemistry
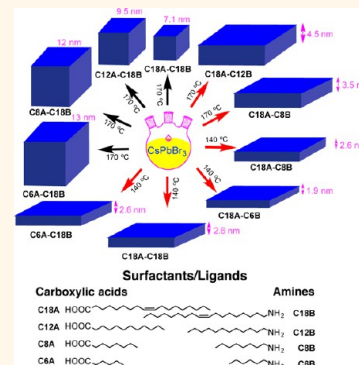
AMX₃ type (A = cation, M = Pb, Sn, X = Cl, Br, I) perovskite materials have attracted surging research interest for their exceptional photovoltaic and optoelectronic characteristics,[1−7] which have led to promising applications such as high-efficiency photovoltaic solar cells,[2−,4,8] light-emitting devices,[9−11] lasers,[12−14] and photodetectors.[15,16] Great effort has been devoted to improving photoelectronic efficiencies in thin films[2−4,8] and understanding fundamental optoelectronic processes in single crystals of organic/inorganic lead halide perovskites.[17−19] The corresponding perovskites containing organic cations such as methylammonium and formamidinium have resulted in single-junction photovoltaic devices with over 20% power conversion efficiency.[1,4,20,21] When reducing the dimension from the bulk to the nanoscale, i.e., in the quantum confined space, the ionic perovskites begin to display extraordinary colloidal properties, including widely tunable absorption and emission ranges, narrow spectral width, high quantum efficiencies, and considerable suppression of photoluminescence (PL) intermittency (blinking).[22] This latest entry of the nanocrystal families distinguishes itself from the
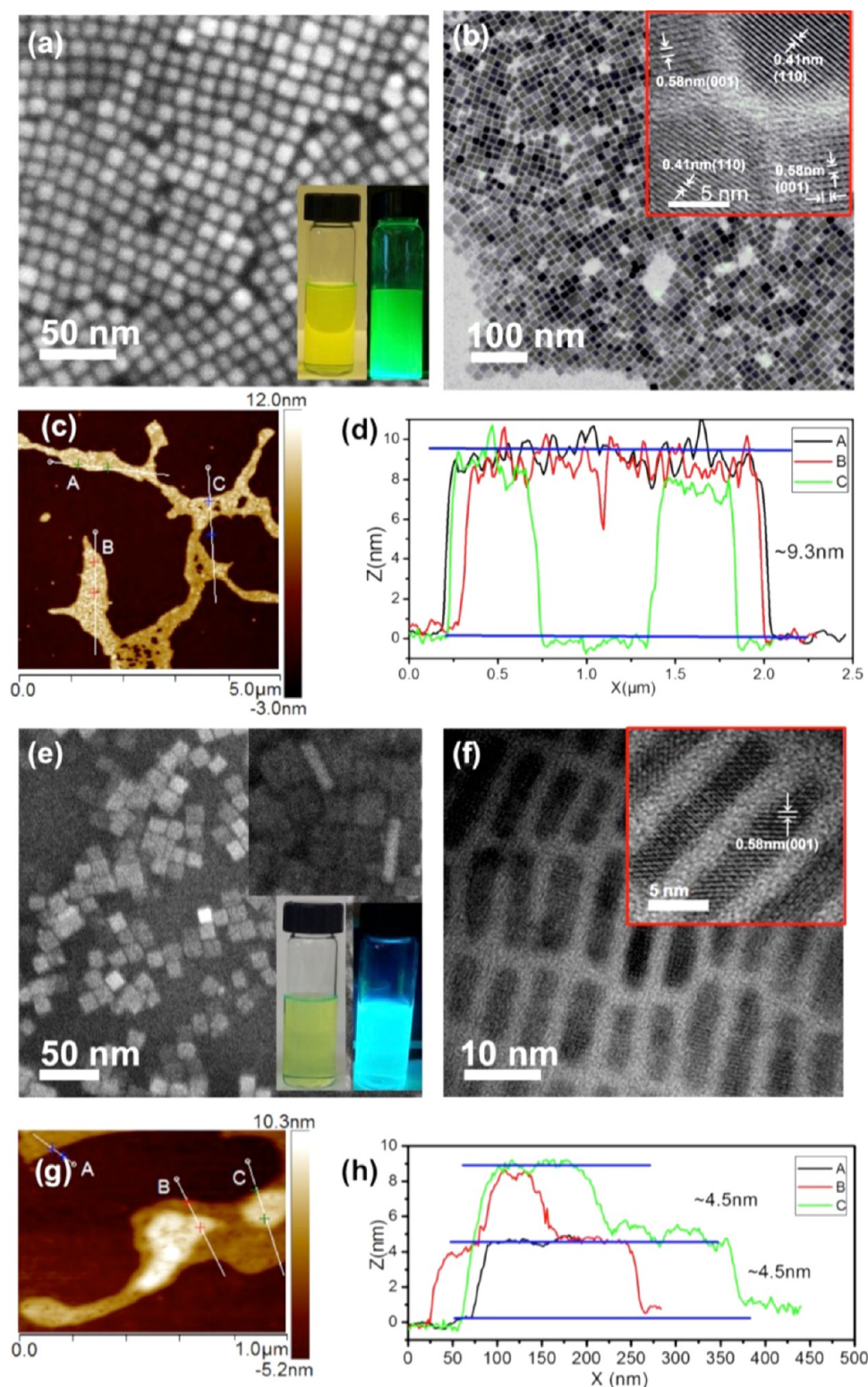
Figure 1. (a) SEM and (b) TEM of CsPbBr$_3$ nanocubes from reactions using oleic acid and oleylamine as ligands and CsOAc as the cesium precursor. Insets in (a): photographs of the colloidal hexane solution of CsPbBr$_3$ nanocubes under room light and UV light. Inset in (b): HR-TEM image showing the crystal lattice information. (c) AFM topography images and (d) line profiles of a submonolayer of CsPbBr$_3$ nanocubes. (e) SEM and (f) TEM of CsPbBr$_3$ nanoplatelets from reactions using oleic acid and oleylamine as ligands and CsOAc as the cesium precursor. Insets in (e): coexisting face-on and edge-on oriented nanoplatelets and photographs of the colloidal hexane solutions of CsPbBr$_3$ nanoplatelets under room and UV light. Inset in (f): HR-TEM image showing the crystal lattice information. (g) AFM topography image and (h) line profiles of layers of CsPbBr$_3$ nanoplatelets.

traditional colloidal semiconductor quantum dots in its ionic nature, which invites more detailed studies toward better

synthetic control and full understanding of their excellent optoelectronic characteristics.

Synthesis of the lead halide perovskite nanocrystals, including both the hybrid organic−inorganic[23−25] and the all-inorganic ones,[26−31] has been realized *via* convenient solution-based procedures, during which shape and size control are exercised through the control of temperature, reaction time, and reaction compositions. Subsequent to the synthesis of organolead halide perovskite nanocrystals pioneered by Schmidt *et al.*,[23] hybrid perovskite nanoplatelets have also been reported,[24,25] the thickness and PL of which could be tuned by varying the organic cations. In the arena of all-inorganic CsPbX$_3$ (X = Cl, Br, I) perovskite nanocrystals, Protesescu *et al.* is among the first to demonstrate the successful synthesis of nanocubes using a hot-injection and fast-cooling approach.[27,28] Most recently all-inorganic perovskite nanowires,[29] nanoplatelets,[26,30,32] spherical dots,[31] and nanorods[31] have been obtained by varying the reaction temperature, time, and the surfactant ligands. Also highly notable are the recent efforts on searching for alternatives to lead-based nanomaterials, which have led to the synthesis of tin-based perovskite nanocrystals.[33]

Organic acids and bases are commonly used surfactants in the synthesis of conventional colloidal quantum dots, which can effectively solvate the inorganic precursors, alter the kinetic pathways to give anisotropically developed nanostructures, and stabilize the final colloidal nanostructures as surface ligands.[34−36] Long-chain organic acids and bases have also been employed universally during the synthesis of inorganic perovskite nanocrystals, with oleic acid and oleylamine being the most common pair of choice.[30,31,37] The role of individual acids and amines on the crystal growth and surface properties of this unique ionic semiconductor however remains poorly understood when compared to the conventional colloidal quantum dot counterparts.[38] The fundamental difference between the ionic and covalent quantum dot systems implies very different nucleation processes and surface interactions, which calls for a thorough study using systematically varied organic acid−base combinations. The crystal structures of organic/inorganic layered perovskites have indicated significant hydrogen-bonding interactions between the edge halide atoms and the ammonium groups,[39] the conjugated acid form of the alkylamine, which are different from the amine−metal coordination interactions in colloidal quantum dots. Recent studies implied[40] that only carboxylates are present on the nanocrystal surface, while De Roo *et al.* has indicated[41] that the perovskite nanocrystal surface is dynamically stabilized with either oleylammonium bromide or oleylammonium oleate. The contradictory observations suggest that the presence of an acid−base pair has a profound impact on the morphology and the optical properties of perovskite nanocrystals, yet the origin of such impact still remains unclear and necessitates a more in-depth study. Herein we have systematically varied the hydrocarbon chain composition of amines and carboxylic acids to investigate the surface chemistry and consequently revealed the dependence of perovskite nanocrystal morphologies on the structures of acid and amine. Solution phase studies on purified nanocrystal samples by ^{1}H NMR and IR spectroscopies have unambiguously confirmed the presence of both carboxylate and alkylammonium ligands on surfaces, with the alkylammonium ligand being much more mobile and susceptible to detachment from the nanocrystal surfaces during polar solvent washes. More strikingly, the chain length variation of carboxylic acids and amines, ranging from 18 carbons down to two carbons, has shown independent correlation to the size and shape of nanocrystals. For nanocrystals synthesized at a relatively higher temperature of 170 °C, a shorter carboxylic acid results in larger size CsPbBr$_3$ nanocubes. On the other hand, when shorter amines are used, thinner CsPbBr$_3$ nanoplatelets are obtained, with the thinnest one reaching only three unit cells in thickness. We have additionally demonstrated that the use of a more soluble cesium acetate (CsOAc) precursor results in enhanced processability and smaller sizes without sacrificing optoelectronic properties. This replacement offers a more versatile recipe for perovskite nanocrystal synthesis that allows the use of low boiling point organic acids and amines bearing shorter carbon chains, which may have important implications for lowering the barrier for carrier transport in optoelectronic processes.

RESULTS AND DISCUSSION

Impact of Using Different Cesium Precursors. Cs$_2$CO$_3$ was used as the cesium precursor in all the previously reported synthetic procedures of cesium lead halide perovskite nano-crystals. It is insoluble in the nonpolar reaction solvent octadecene (ODE) and requires the use of oleic acid as cosolvent. Following an acid metathesis reaction, Cs-oleate is generated and remains soluble at temperatures higher than 100 °C. In order to incorporate organic acids and bases with varying chain lengths, some of which have low boiling points, during the synthesis of perovskite nanocrystals, the reaction thus needs to be performed at lower temperatures. To overcome the solubility issue, we replaced Cs$_2$CO$_3$ precursor with the more organosoluble CsOAc, followed by a comparative study to investigate the impact of this replacement on perovskite nanocrystal synthesis.

Parallel reactions employing the two different Cs salts were carried out under identical conditions, using oleic acid and oleylamine as the acid/base pair. CsOAc has much better solubility than Cs$_2$CO$_3$ in ODE and the ODE/acid mixtures at room temperature (Figure S1). Since reaction temperature plays a critical role in regulating the shape and size of the resulting colloidal nanostructures,[26] the reactions were carried out at two different temperatures, 170 and 140 °C, respectively. From the 170 °C reactions, cuboid nanocrystals were obtained from both CsOAc and Cs$_2$CO$_3$ precursors, and from the reactions carried out at 140 °C, nanoplatelets were obtained instead for both Cs precursors. Figure 1 shows the scanning electron microscopy (SEM) and transmission electron microscopy (TEM) images of the CsPbBr$_3$ nanocubes and nanoplatelets obtained from CsOAc precursors, which are similar in shape to their Cs$_2$CO$_3$ counterparts (SEM and TEM images, Figure S2). The average edge length of CsOAc-derived nanocubes is determined to be 7.1 nm according to TEM analysis, consistent with that from SEM analysis (7.5 nm, Figure S3) but slightly smaller than the 8.4 nm size of the nanocubes synthesized from the Cs$_2$CO$_3$ precursor. From the high-resolution TEM (HR-TEM) images (Figure 1b), *d* spacings of 5.8 and 4.1 Å can be clearly identified, corresponding to the (001) and (110) crystal lattice planes.[31] Atomic force microscopy (AFM) (Figure 1c and d) of a submonolayer spun-cast from a dilute solution of the nanocubes revealed an average height of 9.3 nm, corresponding to the total length of the nanocube plus a top and a bottom layer of surface ligand shells.[42] For the nanoplatelets obtained from lower temperature reactions, the quasi-2D structural features were confirmed by corresponding SEM and TEM studies. As shown in Figure 1e, the SEM image of nanoplatelets obtained from CsOAc precursors revealed nanosized squares
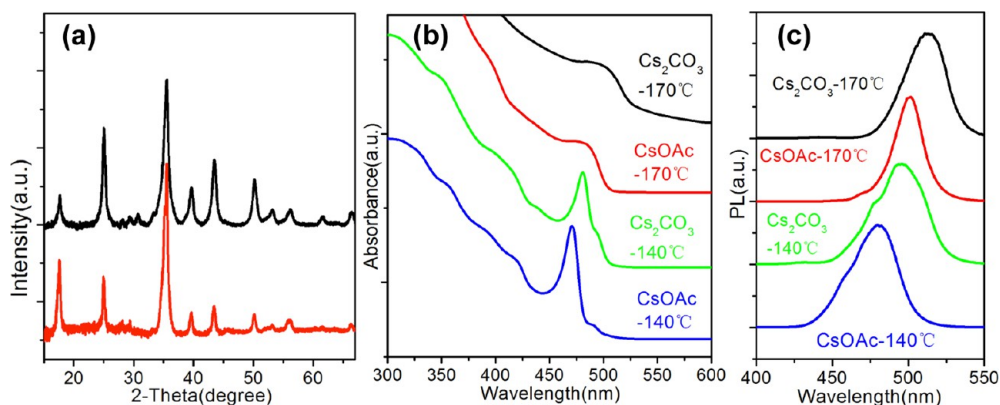
Figure 2. (a) XRD pattern of CsPbBr$_3$ nanocubes (black) and nanoplatelets (red) from CsOAc precursors. (b) Optical absorption and (c) PL emission spectra of CsPbBr$_3$ nanocubes and nanoplatelets from both CsOAc and Cs$_2$CO$_3$ precursors.
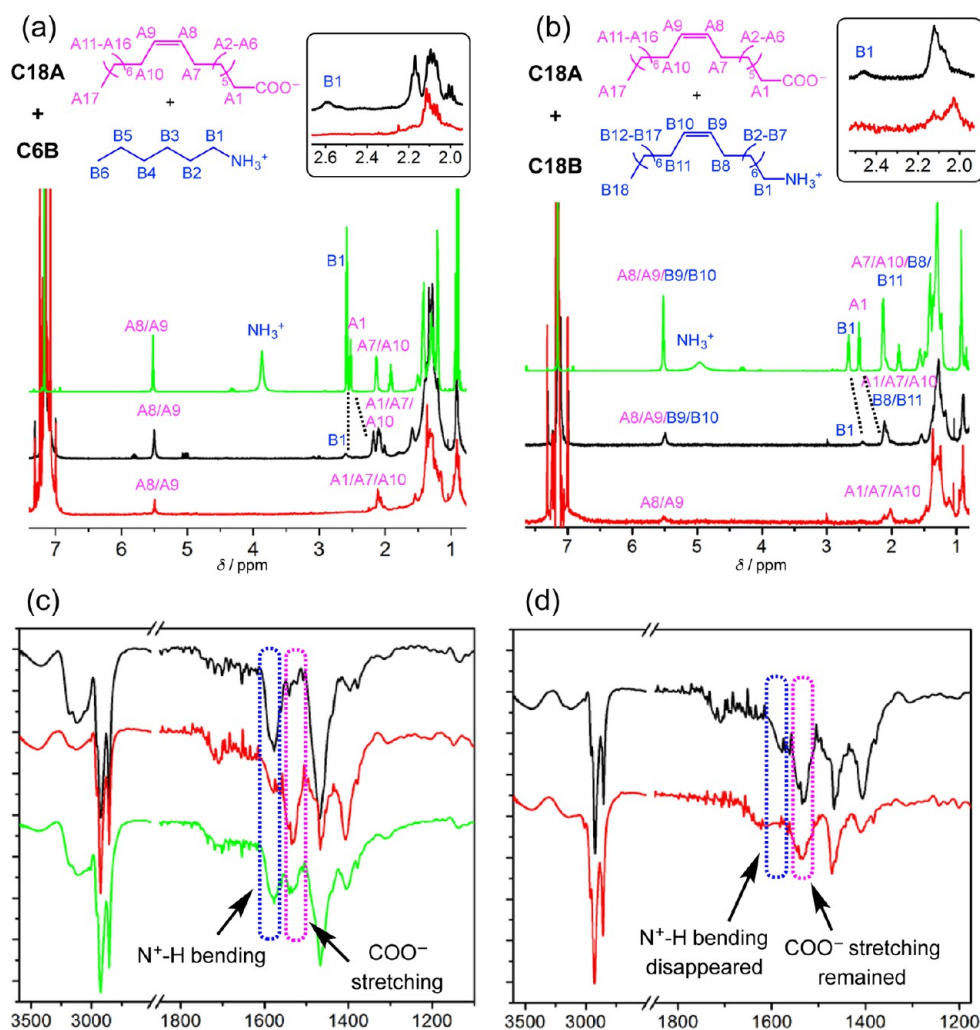
Figure 3. ^{1}H NMR spectra (C$_6$D$_6$, 298 K, 500 MHz) of CsPbBr$_3$ nanocrystals (a) from C18A−C6B after hexane (black) and hexane/acetone wash (red); (b) from C18A−C18B after hexane (black) and hexane/acetone wash (red). The green curves in (a) and (b) are the ^{1}H NMR spectra of mixtures of C18A−C6B and C18A−C18B, respectively, and the boxes in (a) and (b) are the blown-ups of the characteristic changes between wash cycles. (c) IR spectra of CsPbBr$_3$ nanocrystals from C18A−C18B (green), C18A−C6B (red), and C6A−C18B (black). (d) IR spectra of CsPbBr$_3$ nanocrystals washed by hexane (black) and hexane/acetone (red).

with an average edge length of 12.9 nm. From the regions where both face-on and edge-on nanoplatelets were present, the thickness could be determined to be 2.5 nm. TEM studies further confirmed the quasi-2D morphology of these nanoplatelets. The (001) crystal lattice planes could be resolved

from the HR-TEM images,[31] with an average edge length of 12.6 nm and thickness of 2.6 nm, which were very consistent with SEM results (Figure S3). AFM measurements showed (Figure 1g and h) the formation of single layers and bilayers and an average single-layer thickness of 4.5 nm, corresponding

to nanoplatelets coated with two layers of surface ligand shells and similar to the nanocubes obtained from higher temperature reactions. Overall, the combined AFM, SEM, and TEM results provided unequivocal structural evidence for the nanocubic and nanoplatelet morphologies. The bulk crystallinity of the nanocubes and nanoplatelets was also confirmed by powder X-ray diffraction (PXRD) studies (Figure 2a). The peaks at 2θ 17.6°, 25.1°, 35.6°, 39.6°, 43.5°, 50.2°, 53.2°, and 56.2° (Co Kα, 1.79 Å) in the diffractogram could be assigned to the orthorhombic perovskite crystal phase, as was reported recently.[43]

A comparison of the optical properties of the nanocrystals obtained from the two cesium precursors revealed that, on one hand, the cesium precursor substitution results in similarly high photoluminescent internal quantum efficiencies for both nanocubes and nanoplatelets (Table S1); on the other hand, consistent spectroscopic shifts are observed due to the size differences and quantum size effect. As shown in Figure 2b, the absorption onsets of both nanocubes and nanoplatelets from CsOAc were blue-shifted compared to those from Cs$_2$CO$_3$. Similar hypsochromic shifts were also observed for the emission peaks in the PL spectra of CsOAc-based nanocubes and nanoplatelets (Figure 2c).

The successful synthesis of nanocubes and nanoplatelets from both cesium precursors, together with the similar morphologies and optical properties, suggests that despite small size variations there is no fundamental difference during the nucleation and crystallization processes. CsOAc can serve as a reliable cesium precursor with added benefits such as easy manipulation and more compatibility with low-temperature conditions that permit the use of low boiling point reactants. As described later, when oleic acid or oleylamine was replaced with an acid or amine with chain length shorter than eight carbons, no perovskite nanocrystals were formed from reactions using Cs$_2$CO$_3$, which was in strong contrast to CsOAc-based reactions. Therefore, CsOAc is a more versatile precursor that allows systematic variation of synthetic conditions and is employed in all the following perovskite nanocrystal syntheses.

Confirmation of Surface Ligands. It is important to know the surface ligands of CsPbBr$_3$ nanocrystals, as they are strongly related to the shape, size, and optical properties of the nanocrystals. The surface chemistry is also important for introduction of different functionality through subsequent ligand exchange reactions. The reports on the nature of surface ligands on colloidal perovskite nanocrystals however remain ambiguous, most of which lean toward the presence of surface oleates, while the role of oleylamine has not been clarified until very recently. A solution ^{1}H NMR spectroscopic study has identified[41] that both oleylammonium bromide and oleylammonium oleate were under dynamic equilibrium on the surface of CsPbBr$_3$ nanocubes. In that study, however, the authors had to work with large overlapping resonances in ^{1}H NMR spectra since oleylammonium, oleate, and a large excess of ODE solvent have similar alkyl and alkene chain compositions, which potentially obscure the spectral interpretation. The replacement of Cs$_2$CO$_3$ with CsOAc as the cesium precursor allows the use of different combinations of carboxylic acids and amines other than the benchmark oleic acid/oleylamine pair. Organic acid and bases with short and saturated linear alkyl chains were thus introduced during the synthesis, which led to clear separation of characteristic ^{1}H NMR peaks and unambiguous assessment of surface ligands on perovskite nanocrystals. For easy identification of corresponding reactions, we adopted the name

convention CnA−CmB to differentiate various acid−base combinations, in which Cn and Cm denote the number of carbons on the alkyl chains, and A and B denote organic acid and base, respectively.

The CsPbBr$_3$ nanocrystals were worked up from the reactions mixtures by first precipitation with bad solvents, followed by centrifugation at high speed. The supernatants were carefully removed, and the remaining CsPbBr$_3$ solid was subjected to repeated precipitation and centrifugation for up to five cycles in order to remove ODE and remaining excess acid and base. The bad solvents employed to precipitate the CsPbBr$_3$ nanostructures were either pure hexane or a 7:3 (v/v) mixture of hexane and acetone. The isolated CsPbBr$_3$ solid nanocrystals were redispersed in deuterated benzene for ^{1}H NMR spectroscopic studies.

Figure 3a shows stacked ^{1}H NMR spectra of the mixture of C18A−C6B and the CsPbBr$_3$ nanocrystals obtained from C18A−C6B combination and after repeated treatment with hexane or hexane/acetone mixture for five times. A resonance at 5.50 ppm was observed for the two differently washed but otherwise identical samples, which was characteristic for the alkene protons from oleate, indicative of surface-bound oleate on CsPbBr$_3$ nanocrystals. There was an additional characteristic broad resonance at 2.60 ppm in the spectrum of the hexane-washed sample, assignable to the B1 protons in hexylammonium species (see Figure 3 for proton annotations). The broadness of the peaks is strong evidence for the surface-bound state of these ammonium ligands. The B1 protons were absent in the hexane/acetone-washed sample, indicating that the surface-bound ammonium ions were so labile that they were detached from the surface during the polar acetone solvent wash. The remaining oleate resonances in the ^{1}H NMR spectrum suggested that oleate bound much more tightly to the surface and survived the acetone treatment. This solvent-dependent surface ligand binding behavior was consistently observed in samples that were prepared from other acid−amine combinations. Figure 3b shows the stacked ^{1}H NMR spectrum of the mixture of C18A−C18B and of CsPbBr$_3$ nanocrystals obtained from C18A−C18B after different solvent treatment. Both oleate and oleylammonium were clearly present in samples after five hexane washes, as evidenced by the alkene and the B1 resonances. In comparison, the resonance of B1 protons in olelylammonium disappeared in the ^{1}H NMR spectrum of the same sample after five hexane/acetone washes, in accordance with the detachment of surface oleylammonium species. The coexistence of both carboxylates and ammoniums and the disparate stability of surface ligands were further confirmed by ^{1}H NMR spectroscopy of nanocrystals obtained from other acid−base combinations. The stacked ^{1}H NMR spectra of CsPbBr$_3$ nanocrystals obtained from C6A−C18B combination after different solvent treatment are shown in Figure S4a. Olelylammonium was clearly present in the sample that was washed five times with hexane, as evidenced by the alkene resonance at 5.52 ppm. This resonance was markedly reduced after one hexane/acetone wash and disappeared after five washes. Accompanying the loss of the longer olelylammonium surfactant after polar solvent wash was the notably reduced solubility, which resulted in reduced yet discernible signals of hexylate. ^{1}H NMR studies on nanocrystals obtained from the MA−C6B (MA: methacrylic acid, Figure S4b) and C2A−C18B (Figure S4c) reactions all consistently indicated similar binding behavior and solvent responsiveness of carboxylate and ammonium ligands.
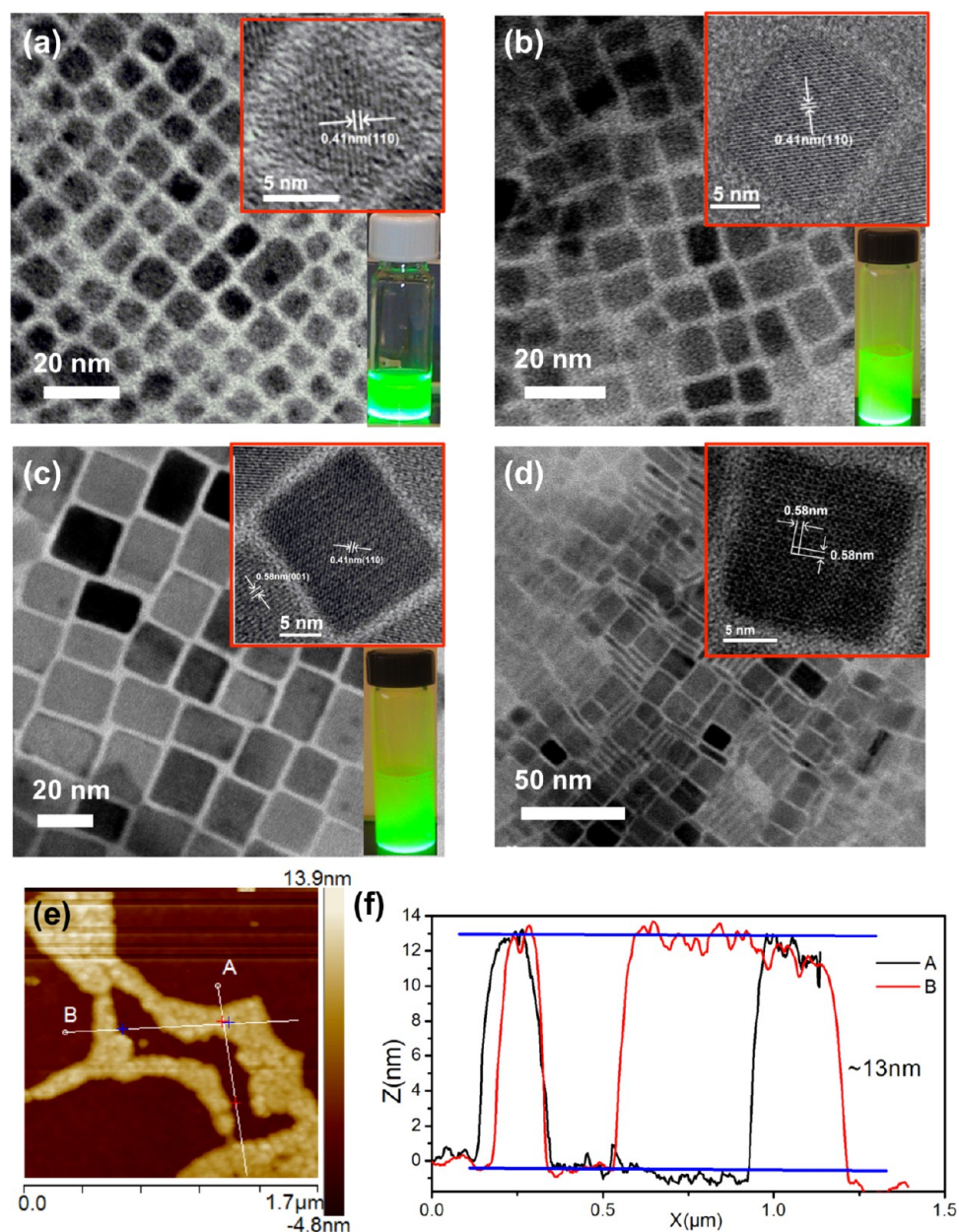
Figure 4. Low- and high-resolution TEM images of CsPbBr$_3$ nanocubes from 170 °C reactions using (a) C12A−C18B, (b) C8A−C18B, and (c) C6A−C18B, respectively. Insets in (a−c): Photographs of CsPbBr$_3$ nanocube colloidal solutions in hexane under UV light. (d) Low- and high-resolution TEM images of CsPbBr$_3$ nanoplatelets from the 140 °C reaction using C6A−C18B. (e) AFM and (f) line profiles of a monolayer film of nanocrystals from C12A−C18B.

Infrared (IR) studies provided consistent evidence that confirmed the solvent dependence of surface ligands. The stacked spectra of hexane-washed nanocrystals from C6A−C18B, C18A−C6B, and C18A−C18B combinations indicate the characteristic carboxylate asymmetric stretching vibration peak at 1545 cm^{-1}, together with the N−H bending vibration peak at 1575 cm^{-1} from ammonium (Figure 3c). Strong C−H bending vibration peaks at 1465 and 1375 cm^{-1} assignable to the hydrocarbon chains from both ligands were also observed. In the IR spectrum of the hexane/acetone-washed nanocrystal samples from C18A−C6B (Figure 3d), peaks corresponding to the ammonium N−H disappeared while those from carboxylate were retained, suggesting the removal of ammonium ions and retention of carboxylates. These results collectively indicate that (a) both carboxylates and ammoniums bind to the nanocrystal surface and (b) ammonium−surface interaction is weaker compared to carboxylate−surface bonding interactions. The disparity of binding strength could be understood by the nature of ligand−surface atom interactions. The carboxylates presumably chelate with surface lead atoms, similar to conventional colloidal quantum dot systems.[44] On the other hand, alkylammonium, instead of alkylamine, interacts with the surface bromide via [Br···H−N$^+$] hydrogen-bonding interactions, as suggested from related crystal structures in hybrid perovskites.[39] The strength of the hydrogen-bonding interaction is weaker compared to metal−ligand coordination and is further reduced in polar solvent medium. As observed in our experiment, the use of acetone readily destabilizes the [Br···H−N$^+$] hydrogen-bonding interaction and dissociates the ammonium from the surface, while oleate binding is much

more robust toward the polar solvent wash. This should be very instructive for further functionalization of the perovksite nanocrystals through ligand exchange.

Surface Ligands' Effect on Morphologies and Optical Properties. The confirmed binding of carboxylate and ammonium ions to the surface of perovskite nanocrystals prompted us to investigate how the different acid−base combinations would affect the growth, final morphology, and optoelectronic properties of the perovskite nanocrystals. In order to rationalize the structural impact of the ligands, we have carried out two series of studies that involve systematic variation of the ligand composition. In each series, the acid or base starting materials were kept as oleic acid or oleylamine, while the counterpart was varied with decreasing chain lengths. The reaction temperatures were either 170 or 140 °C unless otherwise stated. To ensure consistency, all the samples were processed under identical conditions and characterized promptly after purification.

Varying Carboxylic Acids. Perovskite nanocrystals were obtained from the reactions using the same oleylamine and different carboxylic acids including C12A (dodecanoic acid), C8A (octanoic acid), and C6A (hexanoic acid). From these reactions carried out at 170 °C using different acids, crystalline nanocubes were obtained in varying sizes, as revealed by HR-TEM (Figure 4) and SEM (Figure S5). The average edge lengths of nanocubes from C12A−C18B, C8A−C18B, and C6A−C18B combinations from TEM size analysis were approximately 9.5, 12.0, and 13.0 nm (Table 1 and Figure

Table 1. Summary of the Morphology and Optical Properties of Nanostructures Obtained from Different Acid−Base Combinations

sample	temp/°C	morphology	size	PLQY%
C18A−C18B	170	nanocube	7.1 ± 0.8[a]	87%
C18A−C18B	140	nanoplatelet	2.6 ± 0.3[b]	86%
C12A−C18B	170	nanocube	9.5 ± 1.2[a]	63%
C8A−C18B	170	nanocube	12 ± 1.8[a]	55%
C6A−C18B	170	nanocube	13 ± 2.3[a]	59%
C6A−C18B	140	nanoplatelet	2.6 ± 0.4[b]	38%
C2A−C18B	120	nanoplatelet	n.d.[c]	22%
C18A−C12B	170	nanoplatelet	4.5 ± 0.6[b]	51%
C18A−C8B	170	nanoplatelet	3.5 ± 0.4[b]	61%
C18A−C8B	140	nanoplatelet	2.6 ± 0.3[b]	46%
C18A−C6B	140	nanoplatelet	1.8 ± 0.3[b]	36%

[a]Average edge length of nanocube. [b]Average thickness of nanoplatelet. [c]Not determined.

S6), respectively, which were also consistent with those measured by SEM (9.8, 11.8, and 13.0 nm, respectively). Together with the 7.1 nm size nanocubes obtained from the C18A−C18B combination, a correlation is clearly indicated by this series of experiments: decreasing the length of carboxylic acid results in monotonic size increase of the CsPbBr$_3$ perovskite nanocrystals.

The height aspect of the CsPbBr$_3$ nanocubes obtained from the C12A−C18B mixture was further verified by AFM studies (Figure 4e and f), from which a 12.0 nm average height, corresponding to the total thickness of the ligand shells and the nanocube core, was revealed. The crystallinity of these nanocubes was confirmed by the (110) and/or (001) facets observed in HR-TEM and by the bulk measurement using powder XRD (Figure 5a). The diffraction peaks in diffracto-

gram are consistent with the orthorhombic phase of perovskite nanocrystals.[43] The UV−vis absorption and PL properties of these differently sized nanocubes from each acid−base combination indicated progressive red shift of the absorption onset and PL emission peaks of the CsPbBr$_3$ nanocubes as the chain length of the carboxylic acid becomes shorter (Figure 5b and c). The red shift could be understood by the quantum size effect and further confirmed the increasing particle size upon the use of shorter acids. As shown in Table 1, the corresponding quantum yields of the nanocubes are all above 50%.

The reaction using the C6A−C18B combination was separately run at a lower temperature of 140 °C, which resulted in the formation of nanoplatelets. As shown in Figure 4d, both face-on and edge-on nanoplatelets with respect to the substrate were clearly discernible in TEM images, from which an edge length of 20 nm and a thickness of 2.5 nm could be determined. Acetic acid (C2A) was used as the smallest carboxylic acid employed in this series. The reaction temperature was kept at 120 °C in this case in consideration of its low boiling point, which resulted in substantially larger nanoplatelets with wider edge length distribution ranging between 100 and 600 nm (Figure S5).

Varying Amines. In order to investigate the amine effect, we kept the oleic acid (C18A) as the organic acid for all the syntheses but varied the chain length of amines. Saturated alkylamines with 12 (C12B), eight (C8B), and six (C6B) carbons were utilized to replace the oleylamine (C18B) during the synthesis while keeping other conditions the same unless otherwise stated. TEM, HR-TEM (Figure 6), and SEM (Figure S7) studies indicated the formation of nanoplatelets from these reactions carried out at 170 °C using C18A−C12B and C18A−C8B combinations. From the TEM images of C18A−C12B-derived nanoplatelets where both face-on and edge-on samples coexisted (Figure 6a), the edge length and thickness could be determined to be around 20−40 nm and 4.0−4.5 nm, respectively. Thinner nanoplatelets with thicknesses in the range 3−3.5 nm were obtained when shorter octylamine was used (Figure 6b). The formation of nanoplatelets at 170 °C is in direct contrast to oleylamine-based reactions from which only nanocubes were obtained. The reactions were also carried out at a lower temperature at 140 °C for the C18A−C8B and C18A−C6B combinations, from which nanoplatelets with a thickness of 2.5 and 1.9 nm were obtained. AFM studies of a multilayer of the nanoplatelets from C18A−C6B reaction revealed an average height of 3.8 nm, corresponding to a total thickness of the inorganic nanoplatelet core and surface ligand layers (Figure 7a and b). It should be noted that the C18A−C6B-based reaction was not conducted at 170 °C due to the low boiling point of hexylamine. The use of CsOAc is also critical for the successful synthesis of perovskite nanocrystals using amines and acids with six carbons or shorter, as when Cs$_2$CO$_3$ was used instead, only a white precipitate or unstable weakly fluorescent solid was formed instead of yellow colloidal perovskite nanocrystals after the reaction was quenched (Figure S8).

The highly crystalline nature of all the platelets was revealed by HR-TEM (Figure 6) and the bulk PXRD measurement (Figure 7c). (001) and/or (110) crystal lattices were clearly identified from these nanoplatelets. The XRD diffractograms all matched well with the orthorhombic perovskite phase. The nanoplatelets were characterized by their strong blue luminescence (insets in Figure 6) as opposed to the strong
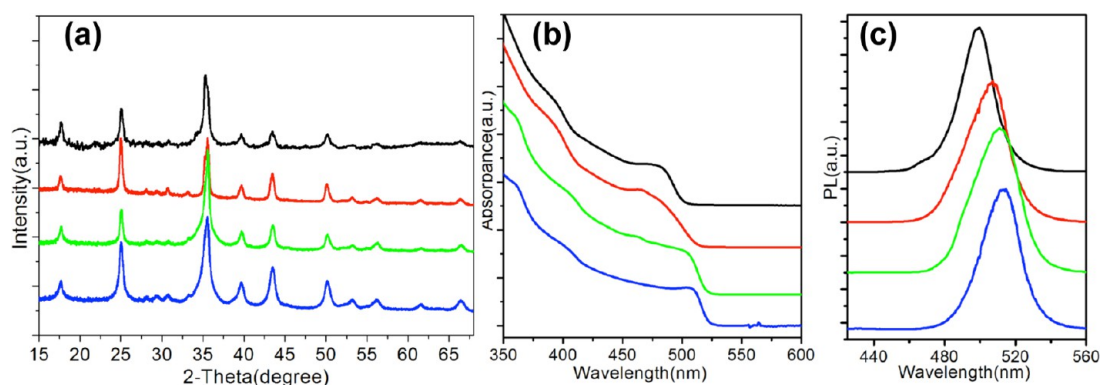
Figure 5. (a) XRD patterns, (b) optical absorption, and (c) PL emission spectra of CsPbBr$_3$ nanocubes synthesized using different acids (black curve: C18A−C18B; red curve: C12A−C18B; green curve: C8A−C18B; blue curve: C6A−C18B).
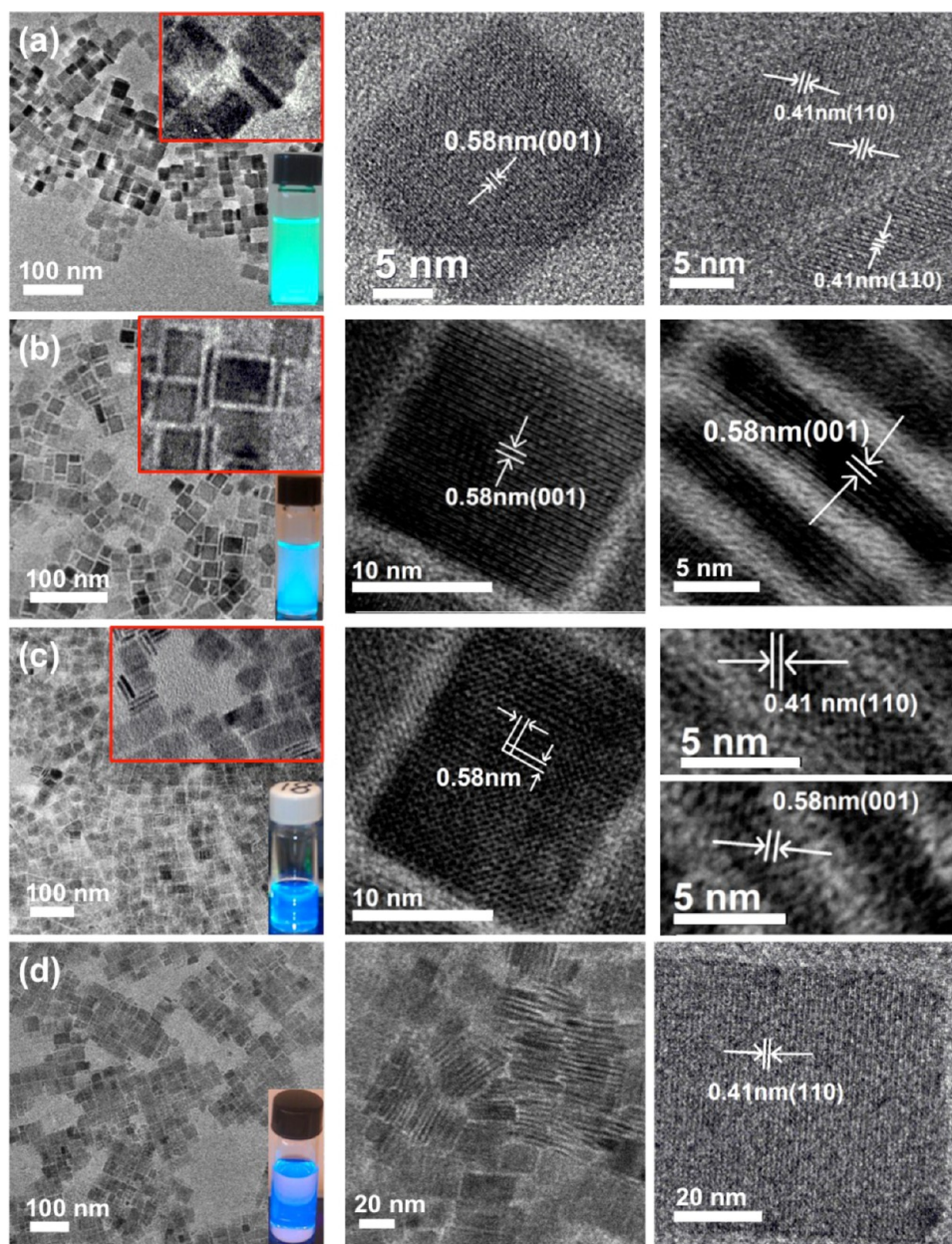

Figure 6. Low- and high-resolution TEM images of CsPbBr$_3$ nanoplatelets from 170 °C reactions using (a) C18A−C12B and (b) C18A−C8B, respectively. Low- and high-resolution TEM images of CsPbBr$_3$ nanoplatelets from 140 °C reactions using (c) C18A−C8B and (d) C18A−C6B. Insets in (a−d): Photographs of CsPbBr$_3$ nanoplatelet colloidal solutions in hexane under UV light.
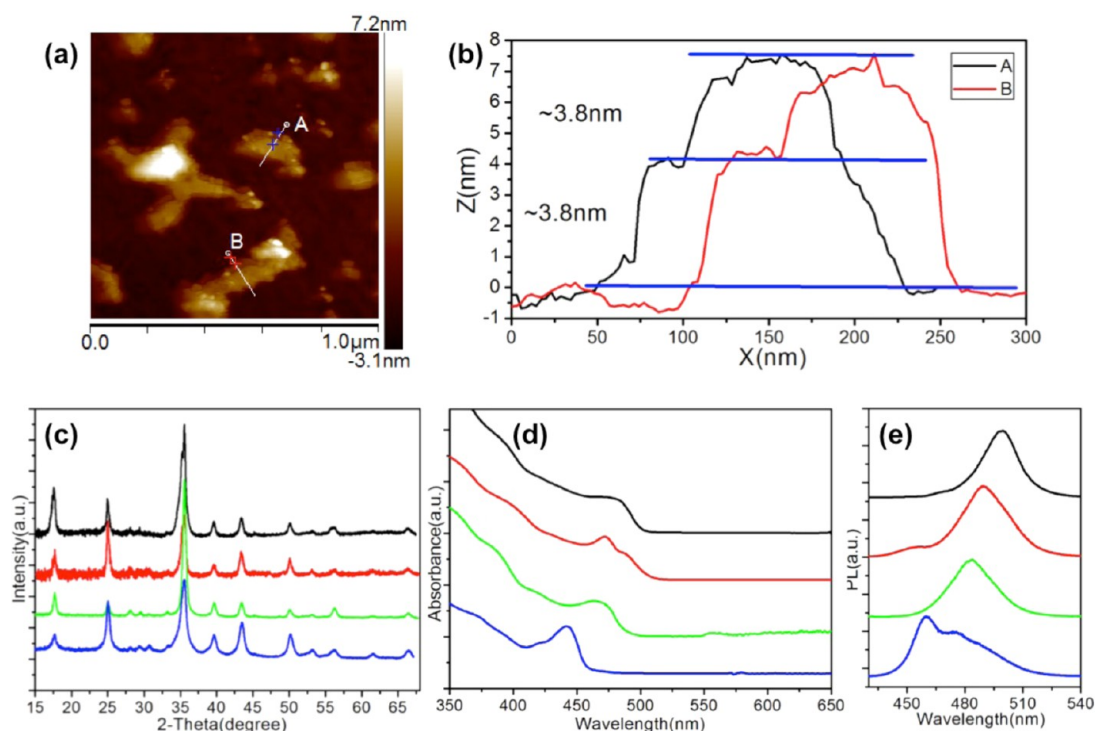
Figure 7. (a) AFM and (b) line profiles of a multilayer of nanocrystals from C18A−C6B. (c) XRD patterns of different CsPbBr$_3$ nanoplatelets synthesized using oleate and different bases (blue: C18B; green: C12B; red: C8B; black: C6B). (d) Optical absorption and (e) PL emission spectra of CsPbBr$_3$ nanocrystals from oleate and different bases (blue: C6B, 140 °C; green: C8B, 170 °C; red: C12B, 170 °C; black: C18B, 170 °C).
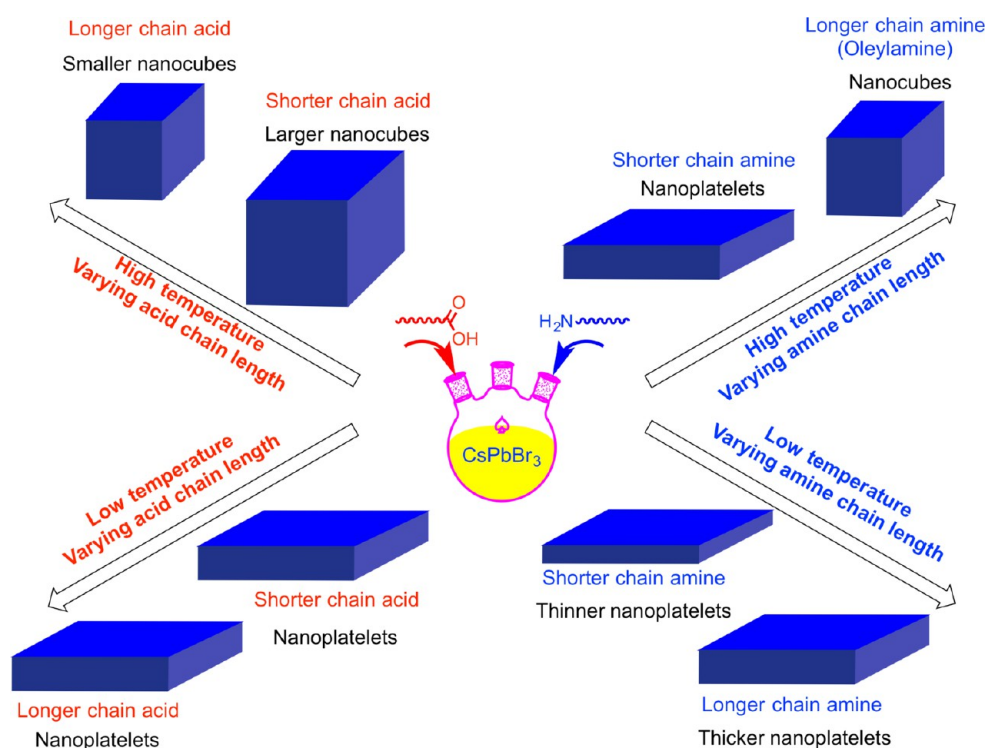

Figure 8. Summary of the shape and size dependence on the chain length of carboxylic acids and amines.

yellow fluorescence associated with nanocubes. Further details were revealed by the UV−vis absorption and PL emission spectra (Figure 7d and e). The nanoplatelets with smaller thicknesses, obtained from shorter chain amines, displayed bluer absorption onsets and emission peaks that are indicative

of quantum size confinement effect. The absorption peaks at 475−490 nm in the spectrum of nanoplatelets from C18A−C12B indicated a thickness of no less than 4 unit cells, and for nanoplatelets from C18A−C8B and C18A−C6B, the absorption peaks at 475 and 450 nm correspond to thicknesses of four

and three unit cells, respectively. The internal PL quantum yields are summarized in Table 1. The quantum yield of the nanoplatelets from the C18A−C8B pair is lower than that of the nanocubes synthesized from the same acid−base combination, a trend that is similar to those synthesized from the C18A−C18B pair.

It was previously discovered that a lower temperature favors the formation of quasi-2D nanoplatelets and a higher temperature favors the formation of nanocubes.[26] We add that the shape selectivity is also dependent on the chain length of amines but less so on the carboxylic acids. As summarized in Figure 8, clear correlations between morphologies and chain length of the ligands are further identified from our studies: the use of shorter chain amines leads to thinner nanoplatelets, and the use of shorter chain carboxylic acids leads to larger size nanocubes from high-temperature reactions.

Although a quantitative description of how the organic surfactant molecules impact the nucleation and crystallization processes in these ionic perovskite nanocrystals is primitive and would require more in-depth modeling and careful kinetic studies, the observed ligand effect does provide qualitative insights into such processes, which presumably involve preferential binding coupled with temperature-dependent dynamic surface−ligand interaction. The shape control during colloidal nanocrystal growth is regarded as a kinetically controlled process, during which high-energy facets grow faster than the low-energy ones to give anisotropic shapes.[35] Both acid and amines are indispensible for the successful synthesis of the perovskite nanocrystals, demonstrating their essential role in coordinating with PbBr$_2$ precursors and the resulting nanocrystals. Selective binding of surfactant ligands to particular facets can decrease their surface energy and accordingly slow their growth. As such binding is dynamic, the surface coverage of these ligands is strongly temperature dependent, allowing dynamic solvation and ligand exchange on and off the surface of growing crystals.[34] Yang *et al.* has suggested preferential binding of oleylamine toward certain facets during the growth of CsPbX$_3$ nanowires.[29] This preferential binding may also be observed during the anisotropic growth of nanoplatelets, where the ammonium competes with Cs$^+$ ions on the surface of the growing platelets and selectively slow the growth along the orthogonal direction.[30] Shorter chain ammonium ions tend to diffuse faster than longer chain ones and, in turn, result in faster on−off exchange rates that lead to more pronounced shape anisotropy and thinner platelets.[36] On the other hand, elevated temperatures may significantly weaken ammonium−surface binding, giving rise to thicker nanoplatelets, or nanocubes in the case of C18A−C18B.

CONCLUSION

We have carried out a comprehensive study to probe the ligand-mediated synthesis of the all-inorganic CsPbBr$_3$ perovskite nanocrystals. Different pairs of carboxylic acids and organic amines with varying chain lengths were utilized during the nanocrystal synthesis, which was further facilitated by the use of CsOAc as the Cs source. CsOAc is proved to be a more versatile precursor than the commonly used Cs$_2$CO$_3$ owing to its greater solubility in the reaction mixture at a broader temperature range, which makes it amenable to conditions that permit the incorporation of more volatile shorter chain acids and amines during the synthesis. The surface ligand compositions were further confirmed by detailed ^{1}H NMR

and IR spectroscopic studies. Both carboxylate and ammonium bind to the surface of the as-synthesized nanocrystals. The final surface ligand composition is however strongly dependent on processing conditions, as the ammonium ligands are prone to be detached from the surface upon the use of more polar acetone during wash cycles, but will remain when nonpolar hexane solvent is used. This confirms that carboxylate ligands bind more strongly to the surface than the ammonium ions do. From reactions carried out at 170 °C using oleylamine and carboxylic acids with decreasing carbon chain lengths, nanocubes with increasing edge lengths were obtained, and from reactions carried out at 170 °C using oleic acid and amines with shorter carbon chain lengths, nanoplatelets were obtained except in the case of oleylamine. The thickness of nanoplatelets also displays a chain-length dependence, as thinner nanoplatelets were produced from shorter chain amines, with the thinnest reaching only three perovskite unit cells. The findings confirm that although ammonium ions bind more weakly compared to carboxylates, they are more effective in tuning the growth of anisotropic platelet structures, while the stronger carboxylate ligands are more effective in modulating the size of the relatively more isotropic nanocubes. These observations shed lights on the roles of acids and amines, which paves the way for further tuning and manipulating the shape, size, and optoelectronic characteristics, all of which are of great relevance to the future applications of this emerging class of materials.

METHODS

Materials. All reagents were purchased from Sigma and Aldrich and used as received without purification. All reagents are at least 99% pure (reagent grade) except oleic acid and oleylamine, which are 90% pure (analytical reagent grade).

Synthesis of CsPbBr$_3$ Nanocubes or Nanoplatelets. CsPbBr$_3$ nanocubes or nanoplates were prepared following a modified procedure.[27,28] ODE (5 mL) and PbBr$_2$ (0.188 mmol, 0.069 g) were loaded into a 25 mL three-neck flask and dried under vacuum for 1 h at 120 °C. Equimolar organic acid and base pairs were premixed with the following stoichiometry: C18A−C18B (oleic acid, 0.50 mL, and oleylamine, 0.50 mL), C12A−C18B (dodecanoic acid, 0.32 g, and oleylamine, 0.50 mL), C18A−C12B (oleic acid, 0.50 mL, and dodecylamine, 0.29 g), C8A−C18B (octanoic acid, 0.25 mL, and oleylamine, 0.50 mL), C18A−C8B (oleic acid, 0.50 mL, and octylamine, 0.26 mL), C6A−C18B (hexanoic acid, 0.20 mL, and oleylamine, 0.50 mL), C18A−C6B (oleic acid, 0.50 mL, and hexylamine, 0.21 mL), C2A−C18B (acetic acid, 0.10 mL, and oleylamine, 0.50 mL), and MA−C18B (methacrylic acid, 0.14 g, and oleylamine, 0.50 mL). The acid/amine mixtures were dried and injected at 120 °C under N$_2$, except for the C2A−C18B and MA−C18B compositions, which were injected at 100 °C due to their low boiling point. It should be noted that both the acid and base have to be present in order for complete dissolution of the PbBr$_2$ solid. After complete dissolution was achieved, the temperature was raised to the desired temperature between 120 and 170 °C, followed by quick injection of the CsOAc/acid mixture (0.4 mL, 0.125 M in ODE). After mixing for 5 s, the reaction mixture was cooled by an ice−water bath. The crude solution was directly transferred to centrifuge tubes and was centrifuged at 3000 round per minute (rpm) to remove large particles. The supernatant was subjected to high-speed centrifugation at 10 000 rpm for 10 min. The precipitate was collected and redispersed in either pure hexane or a hexane/acetone mixture (hexane/acetone = 0.7:0.3 by volume). The centrifugation−redispersion procedure was repeated three to five times, after which the solid precipitate was collected and redispersed in toluene or hexane for further characterization.

Characterization Methods. ^{1}H NMR spectra were recorded on a Bruker Avance II 500 MHz NMR spectrometer operating at a ^{1}H frequency of 500 MHz and equipped with a BBFO-Z probe. Ultraviolet and visible absorption (UV−vis) spectra for colloidal

solutions were collected using a Cary 5000 UV−vis−NIR spectrophotometer. Photoluminescence and quantum yield measurements were collected using a NanoLog spectrofluorometer. PLQYs were estimated according to the standard procedure using appropriate dye molecules for blue, green, and red spectral regions (coumarin 343, fluorescein, and rhodamine 6G). PXRD data were acquired using a Bruker AXS D8 Discover GADDS X-ray diffractometer equipped with a Vantec-500 area detector operated at 35 kV and 40 mA at a wavelength of Co Kα (1.79 Å). TEM and HR-TEM data were acquired on a FEI Tecnai G220 S-TWIN electron microscope operating at 200 kV with a Gatan SC200 CCD camera. AFM images were acquired on a Nanoscope Dimension CSPM5500 atomic force microscope using the tapping mode. SEM images were acquired on a Zeiss Gemini Ultra-55 analytical field emission scanning electron microscope.

ASSOCIATED CONTENT

Ⓢ **Supporting Information**

The Supporting Information is available free of charge on the ACS Publications website at DOI: 10.1021/acsnano.6b03863.

> SEM, TEM, and HR-TEM images of perovskite nanocubes and nanoplatelets from Cs_2CO_3; statistical SEM and TEM analysis of nanocube and nanoplatelet perovskites; ^1H NMR spectra (PDF)

AUTHOR INFORMATION

Corresponding Authors
*E-mail (L. He): heling@mail.xjtu.edu.cn.
*E-mail (Y. Liu): yliu@lbl.gov.

Notes
The authors declare no competing financial interest.

ACKNOWLEDGMENTS

REFERENCES

(1) Chung, I.; Lee, B.; He, J.; Chang, R. P.; Kanatzidis, M. G. All-Solid-State Dye-Sensitized Solar Cells with High Efficiency. *Nature* **2012**, *485*, 486−489.

(2) Burschka, J.; Pellet, N.; Moon, S.-J.; Humphry-Baker, R.; Gao, P.; Nazeeruddin, M. K.; Grätzel, M. Sequential Deposition as a Route to High-Performance Perovskite-Sensitized Solar Cells. *Nature* **2013**, *499*, 316−319.

(3) Green, M. A.; Ho-Baillie, A.; Snaith, H. J. The Emergence of Perovskite Solar Cells. *Nat. Photonics* **2014**, *8*, 506−514.

(4) Hao, F.; Stoumpos, C. C.; Cao, D. H.; Chang, R. P.; Kanatzidis, M. G. Lead-Free Solid-State Organic-Inorganic Halide Perovskite Solar Cells. *Nat. Photonics* **2014**, *8*, 489−494.

(5) Fu, Y.; Meng, F.; Rowley, M. B.; Thompson, B. J.; Shearer, M. J.; Ma, D.; Hamers, R. J.; Wright, J. C.; Jin, S. Solution Growth of Single

Crystal Methylammonium Lead Halide Perovskite Nanostructures for Optoelectronic and Photovoltaic Applications. *J. Am. Chem. Soc.* **2015**, *137*, 5810−5818.

(6) Stoumpos, C. C.; Kanatzidis, M. G. The Renaissance of Halide Perovskites and Their Evolution as Emerging Semiconductors. *Acc. Chem. Res.* **2015**, *48*, 2791−2802.

(7) Seth, S.; Mondal, N.; Patra, S.; Samanta, A. Fluorescence Blinking and Photoactivation of All-Inorganic Perovskite Nanocrystals $CsPbBr_3$ and $CsPbBr_2I$. *J. Phys. Chem. Lett.* **2016**, *7*, 266−271.

(8) Grätzel, M. The Light and Shade of Perovskite Solar Cells. *Nat. Mater.* **2014**, *13*, 838−842.

(9) Tan, Z.-K.; Moghaddam, R. S.; Lai, M. L.; Docampo, P.; Higler, R.; Deschler, F.; Price, M.; Sadhanala, A.; Pazos, L. M.; Credgington, D. Bright Light-Emitting Diodes Based on Organometal Halide Perovskite. *Nat. Nanotechnol.* **2014**, *9*, 687−692.

(10) Song, J.; Li, J.; Li, X.; Xu, L.; Dong, Y.; Zeng, H. Quantum Dot Light−Emitting Diodes Based on Inorganic Perovskite Cesium Lead Halides ($CsPbX_3$). *Adv. Mater.* **2015**, *27*, 7162−7167.

(11) Yantara, N.; Bhaumik, S.; Yan, F.; Sabba, D.; Dewi, H. A.; Mathews, N.; Boix, P. P.; Demir, H. V.; Mhaisalkar, S. Inorganic Halide Perovskites for Efficient Light-Emitting Diodes. *J. Phys. Chem. Lett.* **2015**, *6*, 4360−4364.

(12) Xing, G.; Mathews, N.; Lim, S. S.; Yantara, N.; Liu, X.; Sabba, D.; Grätzel, M.; Mhaisalkar, S.; Sum, T. C. Low-Temperature Solution-Processed Wavelength-Tunable Perovskites for Lasing. *Nat. Mater.* **2014**, *13*, 476−480.

(13) Yakunin, S.; Protesescu, L.; Krieg, F.; Bodnarchuk, M. I.; Nedelcu, G.; Humer, M.; De Luca, G.; Fiebig, M.; Heiss, W.; Kovalenko, M. V. Low-Threshold Amplified Spontaneous Emission and Lasing from Colloidal Nanocrystals of Caesium Lead Halide Perovskites. *Nat. Commun.* **2015**, *6*, 8056.

(14) Eaton, S. W.; Lai, M.; Gibson, N. A.; Wong, A. B.; Dou, L.; Ma, J.; Wang, L.-W.; Leone, S. R.; Yang, P. Lasing in Robust Cesium Lead Halide Perovskite Nanowires. *Proc. Natl. Acad. Sci. U. S. A.* **2016**, *113*, 1993−1998.

(15) Stoumpos, C. C.; Malliakas, C. D.; Peters, J. A.; Liu, Z.; Sebastian, M.; Im, J.; Chasapis, T. C.; Wibowo, A. C.; Chung, D. Y.; Freeman, A. J. Crystal Growth of the Perovskite Semiconductor $CsPbBr_3$: A New Material for High-Energy Radiation Detection. *Cryst. Growth Des.* **2013**, *13*, 2722−2727.

(16) Ramasamy, P.; Lim, D.-H.; Kim, B.; Lee, S.-H.; Lee, M.-S.; Lee, J.-S. All-Inorganic Cesium Lead Halide Perovskite Nanocrystals for Photodetector Applications. *Chem. Commun.* **2016**, *52*, 2067−2070.

(17) Dong, Q.; Fang, Y.; Shao, Y.; Mulligan, P.; Qiu, J.; Cao, L.; Huang, J. Electron-Hole Diffusion Lengths > 175 Mm in Solution-Grown $CH_3NH_3PbI_3$ Single Crystals. *Science* **2015**, *347*, 967−970.

(18) Fang, H.-H.; Raissa, R.; Abdu-Aguye, M.; Adjokatse, S.; Blake, G. R.; Even, J.; Loi, M. A. Photophysics of Organic−Inorganic Hybrid Lead Iodide Perovskite Single Crystals. *Adv. Funct. Mater.* **2015**, *25*, 2378−2385.

(19) Shi, D.; Adinolfi, V.; Comin, R.; Yuan, M.; Alarousu, E.; Buin, A.; Chen, Y.; Hoogland, S.; Rothenberger, A.; Katsiev, K.; Losovyj, Y.; Zhang, X.; Dowben, P. A.; Mohammed, O. F.; Sargent, E. H.; Bakr, O. M. Low Trap-State Density and Long Carrier Diffusion in Organolead Trihalide Perovskite Single Crystals. *Science* **2015**, *347*, 519−522.

(20) Zhou, H.; Chen, Q.; Li, G.; Luo, S.; Song, T.-b.; Duan, H.-S.; Hong, Z.; You, J.; Liu, Y.; Yang, Y. Interface Engineering of Highly Efficient Perovskite Solar Cells. *Science* **2014**, *345*, 542−546.

(21) Dou, L.; Wong, A. B.; Yu, Y.; Lai, M.; Kornienko, N.; Eaton, S. W.; Fu, A.; Bischak, C. G.; Ma, J.; Ding, T.; Ginsberg, N. S.; Wang, L.-W.; Alivisatos, A. P.; Yang, P. Atomically Thin Two-Dimensional Organic-Inorganic Hybrid Perovskites. *Science* **2015**, *349*, 1518−1521.

(22) Swarnkar, A.; Chulliyil, R.; Ravi, V. K.; Irfanullah, M.; Chowdhury, A.; Nag, A. Colloidal $CsPbBr_3$ Perovskite Nanocrystals: Luminescence Beyond Traditional Quantum Dots. *Angew. Chem., Int. Ed.* **2015**, *54*, 15424−15428.

(23) Schmidt, L. C.; Pertegás, A.; González-Carrero, S.; Malinkiewicz, O.; Agouram, S.; Mínguez Espallargas, G.; Bolink, H. J.; Galian, R. E.;

Pérez-Prieto, J. Nontemplate Synthesis of CH$_3$NH$_3$PbBr$_3$ Perovskite Nanoparticles. *J. Am. Chem. Soc.* **2014**, *136*, 850−853.

(24) Sichert, J. A.; Tong, Y.; Mutz, N.; Vollmer, M.; Fischer, S.; Milowska, K. Z.; García Cortadella, R.; Nickel, B.; Cardenas-Daw, C.; Stolarczyk, J. K. Quantum Size Effect in Organometal Halide Perovskite Nanoplatelets. *Nano Lett.* **2015**, *15*, 6521−6527.

(25) Yuan, Z.; Shu, Y.; Xin, Y.; Ma, B. Highly Luminescent Nanoscale Quasi-2D Layered Lead Bromide Perovskites with Tunable Emissions. *Chem. Commun.* **2016**, *52*, 3887−3890.

(26) Bekenstein, Y.; Koscher, B. A.; Eaton, S. W.; Yang, P.; Alivisatos, A. P. Highly Luminescent Colloidal Nanoplates of Perovskite Cesium Lead Halide and Their Oriented Assemblies. *J. Am. Chem. Soc.* **2015**, *137*, 16008−16011.

(27) Nedelcu, G.; Protesescu, L.; Yakunin, S.; Bodnarchuk, M. I.; Grotevent, M. J.; Kovalenko, M. V. Fast Anion-Exchange in Highly Luminescent Nanocrystals of Cesium Lead Halide Perovskites (CsPbX$_3$, X= Cl, Br, I). *Nano Lett.* **2015**, *15*, 5635−5640.

(28) Protesescu, L.; Yakunin, S.; Bodnarchuk, M. I.; Krieg, F.; Caputo, R.; Hendon, C. H.; Yang, R. X.; Walsh, A.; Kovalenko, M. V. Nanocrystals of Cesium Lead Halide Perovskites (CsPbX$_3$, X = Cl, Br, and I): Novel Optoelectronic Materials Showing Bright Emission with Wide Color Gamut. *Nano Lett.* **2015**, *15*, 3692−3696.

(29) Zhang, D.; Eaton, S. W.; Yu, Y.; Dou, L.; Yang, P. Solution-Phase Synthesis of Cesium Lead Halide Perovskite Nanowires. *J. Am. Chem. Soc.* **2015**, *137*, 9230−9233.

(30) Akkerman, Q. A.; Motti, S. G.; Srimath Kandada, A. R.; Mosconi, E.; D'Innocenzo, V.; Bertoni, G.; Marras, S.; Kamino, B. A.; Miranda, L.; De Angelis, F. Colloidal Cesium Lead Halide Perovskite Nanoplatelets with Monolayer-Level Thickness Control by a Solution Synthesis Approach. *J. Am. Chem. Soc.* **2016**, *138*, 1010−1016.

(31) Sun, S.; Yuan, D.; Xu, Y.; Wang, A.; Deng, Z. Ligand-Mediated Synthesis of Shape-Controlled Cesium Lead Halide Perovskite Nanocrystals *via* Reprecipitation Process at Room Temperature. *ACS Nano* **2016**, *10*, 3648−3657.

(32) Shamsi, J.; Dang, Z.; Bianchini, P.; Canale, C.; Stasio, F. D.; Brescia, R.; Prato, M.; Manna, L. Colloidal Synthesis of Quantum Confined Single Crystal CsPbBr$_3$ Nanosheets with Lateral Size Control up to the Micrometer Range. *J. Am. Chem. Soc.* **2016**, *138*, 7240−7243.

(33) Jellicoe, T. C.; Richter, J. M.; Glass, H. F. J.; Tabachnyk, M.; Brady, R.; Dutton, S. E.; Rao, A.; Friend, R. H.; Credgington, D.; Greenham, N. C.; Böhm, M. L. Synthesis and Optical Properties of Lead-Free Cesium Tin Halide Perovskite Nanocrystals. *J. Am. Chem. Soc.* **2016**, *138*, 2941−2944.

(34) Yin, Y.; Alivisatos, A. P. Colloidal Nanocrystal Synthesis and the Organic-Inorganic Interface. *Nature* **2005**, *437*, 664−670.

(35) Bealing, C. R.; Baumgardner, W. J.; Choi, J. J.; Hanrath, T.; Hennig, R. G. Predicting Nanocrystal Shape through Consideration of Surface-Ligand Interactions. *ACS Nano* **2012**, *6*, 2118−2127.

(36) Pradhan, N.; Xie, R.; Aldana, J.; Peng, X.; Reifsnyder, D. Surface Ligand Dynamics in Growth of Nanocrystals. *J. Am. Chem. Soc.* **2007**, *129*, 9500−9509.

(37) Wolcott, A.; Doyeux, V.; Nelson, C. A.; Gearba, R.; Lei, K. W.; Yager, K. G.; Dolocan, A. D.; Williams, K.; Nguyen, D.; Zhu, X.-Y. Anomalously Large Polarization Effect Responsible for Excitonic Red Shifts in PbSe Quantum Dot Solids. *J. Phys. Chem. Lett.* **2011**, *2*, 795−800.

(38) Boles, M. A.; Ling, D.; Hyeon, T.; Talapin, D. V. The Surface Science of Nanocrystals. *Nat. Mater.* **2016**, *15*, 141−153.

(39) Sourisseau, S.; Louvain, N.; Bi, W.; Mercier, N.; Rondeau, D.; Boucher, F.; Buzaré, J.-Y.; Legein, C. Reduced Band Gap Hybrid Perovskites Resulting from Combined Hydrogen and Halogen Bonding at the Organic−Inorganic Interface. *Chem. Mater.* **2007**, *19*, 600−607.

(40) Kim, Y.; Yassitepe, E.; Voznyy, O.; Comin, R.; Walters, G.; Gong, X.; Kanjanaboos, P.; Nogueira, A. F.; Sargent, E. H. Efficient Luminescence from Perovskite Quantum Dot Solids. *ACS Appl. Mater. Interfaces* **2015**, *7*, 25007−25013.

(41) De Roo, J.; Ibáñez, M.; Geiregat, P.; Nedelcu, G.; Walravens, W.; Maes, J.; Martins, J. C.; Van Driessche, I.; Kovalenko, M. V.; Hens, Z. Highly Dynamic Ligand Binding and Light Absorption Coefficient of Cesium Lead Bromide Perovskite Nanocrystals. *ACS Nano* **2016**, *10*, 2071−2081.

(42) Schliehe, C.; Juarez, B. H.; Pelletier, M.; Jander, S.; Greshnykh, D.; Nagel, M.; Meyer, A.; Foerster, S.; Kornowski, A.; Klinke, C.; Weller, H. Ultrathin PbS Sheets by Two-Dimensional Oriented Attachment. *Science* **2010**, *329*, 550−553.

(43) Cottingham, P.; Brutchey, R. L. On the Crystal Structure of Colloidally Prepared CsPbBr$_3$ Quantum Dots. *Chem. Commun.* **2016**, *52*, 5246−5249.

(44) Zherebetskyy, D.; Scheele, M.; Zhang, Y.; Bronstein, N.; Thompson, C.; Britt, D.; Salmeron, M.; Alivisatos, P.; Wang, L.-W. Hydroxylation of the Surface of PbS Nanocrystals Passivated with Oleic Acid. *Science* **2014**, *344*, 1380−1384.